

Article

Facile Route for Fabrication of Ferrimagnetic Mn_3O_4 Spinel Material for Supercapacitors with Enhanced Capacitance

Wenjuan Yang, Mohamed Nawwar  and Igor Zhitomirsky * 

Department of Materials Science and Engineering, McMaster University, Hamilton, ON L8S4L7, Canada; yangw48@mcmaster.ca (W.Y.); nawwarm@mcmaster.ca (M.N.)

* Correspondence: zhitom@mcmaster.ca

Abstract: The purpose of this investigation was the development of a new colloidal route for the fabrication of Mn_3O_4 electrodes for supercapacitors with enhanced charge storage performance. Mn_3O_4 -carbon nanotube electrodes were fabricated with record-high capacitances of 6.67 F cm^{-2} obtained from cyclic voltammetry tests at a scan rate of 2 mV s^{-1} and 7.55 F cm^{-2} obtained from the galvanostatic charge–discharge tests at a current density of 3 mA cm^{-2} in $0.5 \text{ M Na}_2\text{SO}_4$ electrolyte in a potential window of 0.9 V . The approach involves the use of murexide as a capping agent for the synthesis of Mn_3O_4 and a co-dispersant for Mn_3O_4 and carbon nanotubes. Good electrochemical performance of the electrode material was achieved at a high active mass loading of 40 mg cm^{-2} and was linked to a reduced agglomeration of Mn_3O_4 nanoparticles and efficient co-dispersion of Mn_3O_4 with carbon nanotubes. The mechanisms of murexide adsorption on Mn_3O_4 and carbon nanotube are discussed. With the proposed method, the time-consuming electrode activation procedure for Mn_3O_4 electrodes can be avoided. The approach developed in this investigation paves the way for the fabrication of advanced cathodes for asymmetric supercapacitors and multifunctional devices, combining capacitive, magnetic, and other functional properties.



Citation: Yang, W.; Nawwar, M.; Zhitomirsky, I. Facile Route for Fabrication of Ferrimagnetic Mn_3O_4 Spinel Material for Supercapacitors with Enhanced Capacitance. *Energies* **2022**, *15*, 1812. <https://doi.org/10.3390/en15051812>

Academic Editor: Sunkara Srinivasa Rao

Received: 26 January 2022

Accepted: 26 February 2022

Published: 1 March 2022

Publisher's Note: MDPI stays neutral with regard to jurisdictional claims in published maps and institutional affiliations.



Copyright: © 2022 by the authors. Licensee MDPI, Basel, Switzerland. This article is an open access article distributed under the terms and conditions of the Creative Commons Attribution (CC BY) license (<https://creativecommons.org/licenses/by/4.0/>).

Keywords: manganese oxide; carbon nanotube; electrode; supercapacitor; capping agent; synthesis; dispersant

1. Introduction

In recent years, advanced materials have emerged for energy storage in supercapacitors, including metal oxides, conductive polymers, graphene, and other carbon materials, MXenes, complex hydroxides, and composites [1–7]. Oxide materials such as MnO_2 , Fe_3O_4 , BiMn_2O_5 , and V_2O_3 are increasingly being explored due to their large potential windows and high capacitance [6]. Spinel-type oxide materials have generated significant interest due to their promising performance and beneficial materials science aspects [8–11]. Atoms of transition metal elements with different valence states were incorporated into the spinel structure and exhibited redox behavior, imparting advanced pseudocapacitive properties to the spinel oxides [8,12–14]. A large pool of spinel oxides provides a basis for the fabrication of spinel solid solutions with advanced properties [15]. Solid solutions allow a significant improvement in functional properties of materials by a controlled variation in their composition. Solid solutions are widely utilized in energy storage and other fields and often outperform individual spinel oxides for various applications [16–19]. Spinel materials are of particular interest because they exhibit advanced magnetic, catalytic, and other properties and can be used for the fabrication of multifunctional materials [14,20–24]. Mn_3O_4 is a spinel-type ferrimagnetic material that is widely used for the fabrication of advanced spinel solid solutions with enhanced magnetization, catalytic, and energy storage properties in batteries [25–27]. However, the potential of Mn_3O_4 for supercapacitor technology is only beginning to be recognized [28,29]. Mn_3O_4 can potentially outperform MnO_2 , which is currently one of the best materials for cathodes of asymmetric supercapacitors.

The use of Mn_3O_4 offers many advantages for supercapacitor technology compared to MnO_2 . The modification of composition and properties of MnO_2 presents difficulties because of the limited possibility of this oxide to form solid solutions. The low electrical conductivity of MnO_2 is detrimental for applications of this material in supercapacitors. In contrast, Mn_3O_4 can form solid solutions with enhanced conductivity and other functional properties. The fabrication of MnO_2 nanoparticles of controlled size and modification of their morphology generates problems attributed to the use of permanganate precursors for the MnO_2 synthesis. Such precursors react with dispersants, which are critically important for control of particle size, shape, and prevention of agglomeration during synthesis. In contrast, Mn_3O_4 can be synthesized from aqueous solutions of Mn^{2+} salts in the presence of dispersants.

Previous investigations [6] have showed that the capacitance of Mn_3O_4 is significantly lower than that of MnO_2 . However, a significant increase in the capacitance of Mn_3O_4 was observed during cycling [30–33]. Numerous XPS studies revealed oxidation of Mn^{2+} and Mn^{3+} ions on the Mn_3O_4 particle surface during cycling and linked this process to the capacitance increase [31,33–35]. The application of Mn_3O_4 for supercapacitors requires the use of time-consuming activation procedures [31,33,35]. The problems related to applications of Mn_3O_4 in cathodes of supercapacitors can be addressed using dispersing agents for the synthesis of nanoparticles.

This investigation was motivated by the strong potential of Mn_3O_4 spinel material for the fabrication of supercapacitors and multifunctional devices. The goal of this investigation was the fabrication of Mn_3O_4 cathodes for supercapacitors with an enhanced capacitance using murexide as a new capping and dispersion agent. An additional goal was the elimination of the time-consuming activation procedure, which limits practical applications of Mn_3O_4 for supercapacitors. For the first time, we demonstrated that murexide can be used as a dispersant for inorganic nanoparticles and carbon nanotubes. The approach developed in this investigation involved the use of advanced techniques for a wet chemical synthesis and colloidal processing of Mn_3O_4 -carbon nanotube electrodes with high capacitance. We describe the advantages of the murexide dispersant, which allowed for strong tridentate bonding to the particle surface and facilitated electrostatic dispersion. Building on this insight, new chelating dispersants can be used for advanced colloidal nanofabrication technologies. The use of murexide offered benefits for the fabrication of Mn_3O_4 -carbon nanotube electrodes because murexide allowed co-dispersion of Mn_3O_4 and carbon nanotubes, which served as conductive additives. The approach of this investigation resulted in an enhanced electrode performance at a high active mass loading, which is critical for practical applications. In this approach, a record high capacitance of Mn_3O_4 electrodes was achieved, and the problems related to capacitance variation during initial cycling were avoided. This eliminated the need for the preparation of Mn_3O_4 based electrodes in time-consuming activation procedures. The results of this investigation open the door for the application of Mn_3O_4 and its solid solutions for energy storage in advanced supercapacitors and multifunctional energy storage devices.

2. Materials and Methods

2.1. Raw Materials

Murexide, $\text{Mn}(\text{NO}_3)_2 \cdot 4\text{H}_2\text{O}$, Na_2SO_4 , NaOH , ethanol, poly(vinyl butyral) (PVB, MilliporeSigma, Oakville, ON, Canada) and multiwalled carbon nanotubes (MWCNTs, Bayer, Leverkusen, Germany) were used as starting materials.

2.2. Synthesis of Mn_3O_4 and Electrode Fabrication

Mn_3O_4 nanoparticles were prepared by a modified chemical precipitation method [30] and mixed with MWCNTs. A solution of 0.33 g of $\text{Mn}(\text{NO}_3)_2 \cdot 4\text{H}_2\text{O}$ in DI water was prepared, and then the pH of the solution was increased to $\text{pH} = 10$ with aqueous NaOH for the Mn_3O_4 synthesis. In method 1, the synthesized Mn_3O_4 was mixed with MWCNTs, and murexide was added as a co-dispersant. In method 2, murexide was added to $\text{Mn}(\text{NO}_3)_2$

solution in DI water before pH adjustment as a capping agent for synthesis, and MWCNTs were added after the synthesis. In both methods, Mn_3O_4 and MWCNTs were co-dispersed using murexide. The mass ratio of Mn_3O_4 :CNT:murexide was 4:1:1. The obtained mixtures of Mn_3O_4 with MWCNTs, containing murexide, were ultrasonicated to achieve improved dispersion and mixing, washed, and dried. Obtained powders were used for the fabrication of electrodes using slurries of Mn_3O_4 and MWCNTs in ethanol with a PVB binder. The binder content was 3% of the total mass of Mn_3O_4 and MWCNTs. The slurries were used for impregnation of commercial Ni foam (Vale, Canada) current collectors. The total mass of impregnated material after drying was 40 mg cm^{-2} .

2.3. Characterization Techniques

Electron microscopy studies were performed using a JEOL SEM (scanning electron microscope, JEOL, JSM-7000F). X-ray diffraction (XRD) analysis (diffractometer Bruker D8, UK) was performed using $\text{Cu-K}\alpha$ radiation at the rate of 0.01 degrees per second. Electrochemical studies were performed in an aqueous 0.5 M Na_2SO_4 electrolyte using PARSTAT 2273 (Ametek) potentiostat for cyclic voltammetry (CV) and electrochemical impedance spectroscopy (EIS), and BioLogic VMP 300 potentiostat for the galvanostatic charge-discharge (GCD) investigations. Testing was performed using a 3-electrode electrochemical cell containing a working electrode (impregnated Ni foam), counter-electrode (Pt mesh), and reference electrode (SCE, saturated calomel electrode). The capacitive properties of electrode material were presented in gravimetric ($C_m, \text{F g}^{-1}$) and areal ($C_s, \text{F cm}^{-2}$) capacitance forms. Capacitances C_m and C_s were calculated from the CV, EIS, and GCD data as described in reference [6]. The capacitances calculated from the CV and GCD data represented the integral capacitances measured in a voltage window of 0–0.9 V versus SCE. The capacitances calculated from the EIS data represented differential capacitances measured at an open circuit potential at a voltage amplitude of 5 mV. CV testing procedures (TP) involved obtaining CV at scan rates of 2, 5, 10, 20, 50, and 100 mV s^{-1} . EIS measurements were performed after each TP. GCD measurements were performed after the last TP.

3. Results and Discussion

Figure 1 shows X-ray diffraction patterns of Mn_3O_4 prepared by methods 1 and 2. The diffraction patterns show peaks of Mn_3O_4 and MWCNTs.

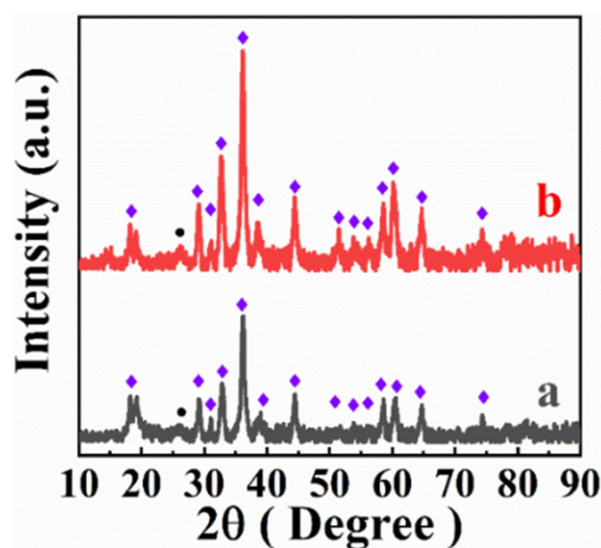


Figure 1. X-ray diffraction patterns of Mn_3O_4 and MWCNT mixtures prepared by (a) method 1 and (b) method 2, (◆- Mn_3O_4 , ●-MWCNT).

The approach developed in this investigation was based on colloidal processing, which offers benefits for the fabrication of materials with advanced microstructures [36–39]. In colloidal processing methods, advanced capping agents and dispersants are necessary for the synthesis of nanomaterials and the fabrication of advanced composites. Capping agents and dispersants must be adsorbed on the particles. A non-adsorbed ionic species can stimulate particle agglomeration. Previous investigations [40] highlighted the benefits of chelating dispersants, which are strongly adsorbed on inorganic particles by bidentate bonding to the surface metal atoms. Figure 2A shows a chemical structure of murexide used in this investigation as a capping and dispersing agent.

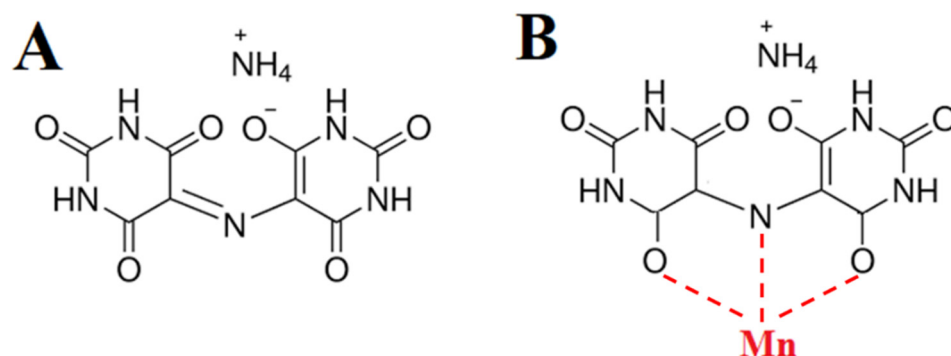


Figure 2. (A) Chemical structure of murexide, (B) adsorption of murexide on particle, involving tridentate chelation of surface Mn atoms.

Murexide exhibits chelating properties [41,42], which are related to its strong tridentate bonding to different metal atoms. Dissociated murexide acquires a negative charge in solutions (Figure 2). It was hypothesized that murexide was adsorbed on the Mn_3O_4 surface by creating a tridentate bonding to Mn atoms on the surface (Figure 2B). The adsorption of murexide on MWCNTs involved interactions [43] of two barbiturate rings of murexide with carbon rings of MWCNTs. The adsorbed murexide imparted a negative charge to the Mn_3O_4 particles and MWCNTs for their electrostatic co-dispersion. It should be noted that many commercial dispersants allow for the dispersion of only inorganic particles or carbon materials. In contrast, murexide allows for the dispersion of both Mn_3O_4 and MWCNTs, facilitating their efficient co-dispersion and mixing.

In this investigation, MWCNTs were used as conductive additives. Previous investigations of as-received MWCNT powders showed that MWCNTs formed large agglomerates with a typical size of 0.5 μm [44]. Therefore, efficient dispersion of MWCNTs was critically important for the fabrication of nanocomposites. Figure 3 shows SEM images of the electrodes prepared by Methods 1 and 2. The SEM images at low magnification show the porous structure of electrodes (Figure 3A,B). The images at higher magnification (Figure 3C,D) show that the size of primary Mn_3O_4 particles was below 100 nm. MWCNTs were distributed between the Mn_3O_4 particles, which was beneficial for the enhancement of electronic conductivity of the composite.

The electrodes prepared by Methods 1 and 2 were tested in 0.5 M Na_2SO_4 electrolyte. Figure 4 shows CVs for the electrodes prepared by Method 1 for different TPs. The CVs obtained at low sweep rates were nearly rectangular. The comparison of the CVs obtained at the same sweep rates for different TPs showed that the area of CV increased with increasing TP number.

This is in agreement with previous investigations, which showed a capacitance increase during cycling [30–33]. Several previous XPS investigations showed an oxidation of Mn^{2+} and Mn^{3+} ions with an increased content of Mn^{4+} ions on the Mn_3O_4 particle surface during cycling and linked this process to the capacitance increase [31,33–35]. Moreover, previous investigations showed that the application of Mn_3O_4 for supercapacitors requires the use of time-consuming activation procedures [31,33,35]. Such procedures are detrimental for practical applications of Mn_3O_4 in supercapacitors.

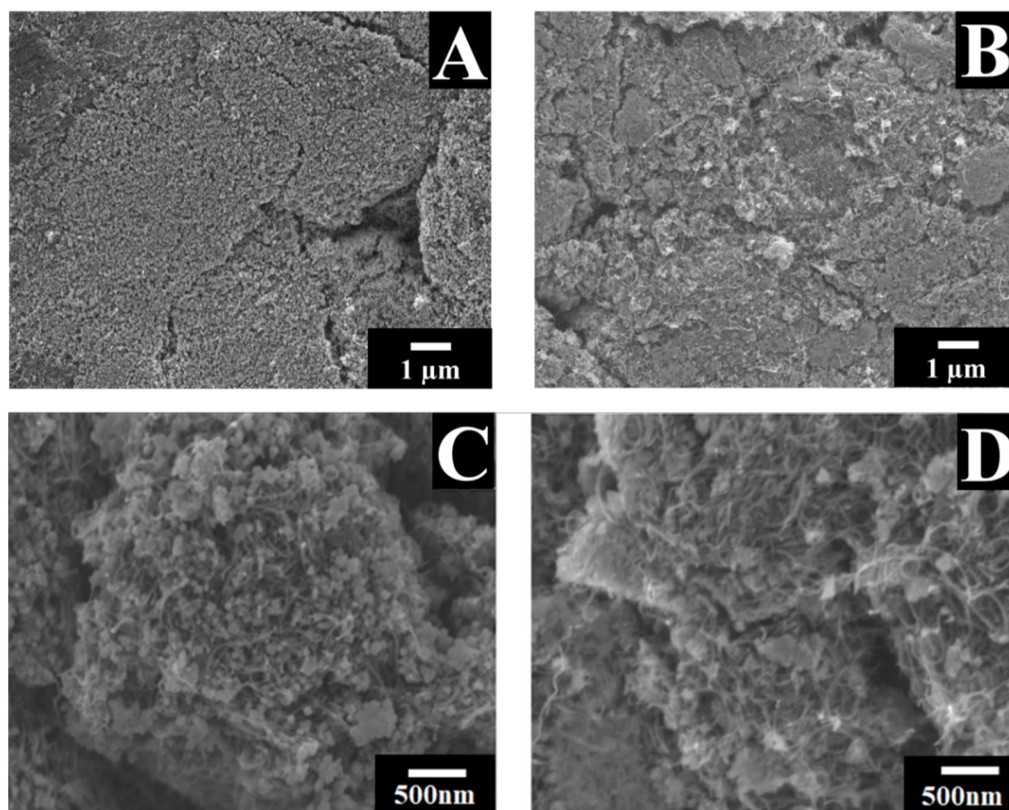


Figure 3. SEM images at different magnifications for electrodes prepared by (A,C) method 1 and (B,D) method 2.

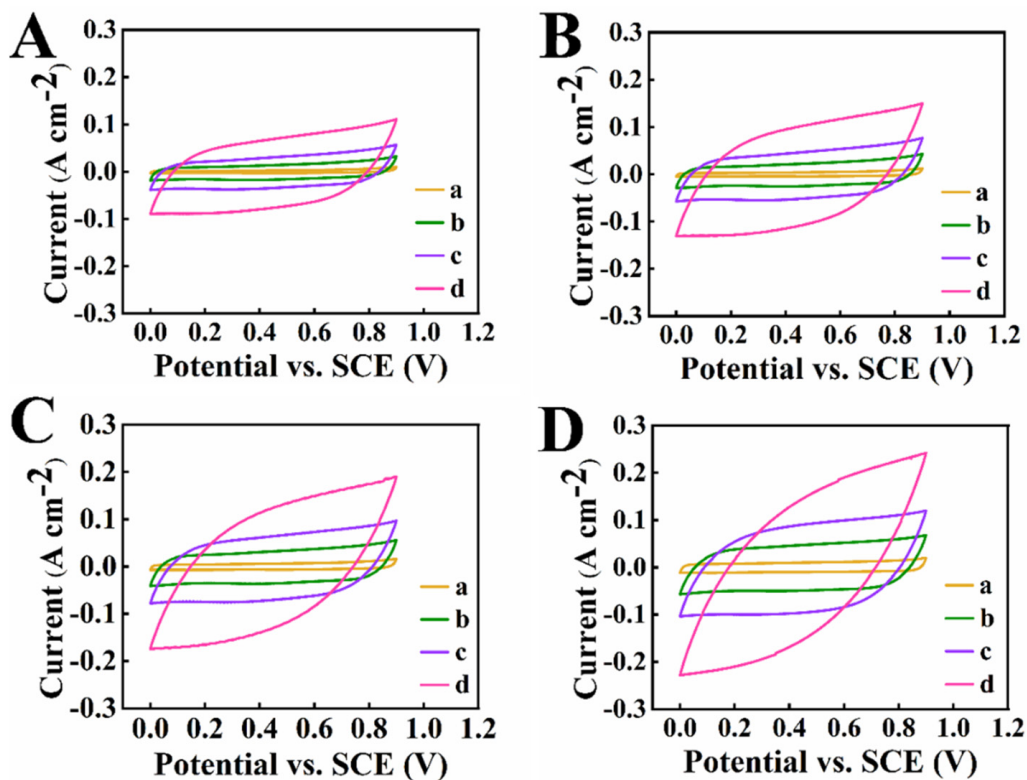


Figure 4. CVs for electrodes, prepared by method 1 for (A) TP 1, (B) TP 2, (C) TP 3 and (D) TP 5 at scan rates of (a) 2, (b) 10, (c) 20 and (d) 50 mV s^{-1} .

It should be noted that we investigated electrodes with high active mass loadings of 40 mg cm^{-2} . In this investigation, commercial Ni foam current collectors were used, which were designed for batteries and supercapacitors, based on inorganic active materials with a typical electrode mass of $30\text{--}50 \text{ mg cm}^{-2}$. High active mass loading is important for practical applications for reducing the contribution of current collectors and other passive components to the total electrode mass. An active mass of about 10 mg cm^{-2} is required for commercial activated carbon electrodes [6,45]. Inorganic materials, such as Mn_3O_4 , have a significantly higher density than the density of activated carbon. Therefore, larger mass loadings can be achieved at the same electrode volume.

The higher gravimetric capacitance of Mn_3O_4 and the higher active mass can potentially result in significantly higher capacitances of Mn_3O_4 -based electrodes, compared to activated carbon electrodes of the same volume. However, it is challenging to achieve good electrode performance at a high active mass. It is known that gravimetric capacitance drops with active mass increase [6]. Moreover, the use of electrodes with high active mass loading aggravated the problem of Mn_3O_4 electrode activation, compared to the thin-film Mn_3O_4 electrodes. This is attributed to better electrolyte access to thin film electrodes, compared to the bulk electrodes with high active mass.

Figure 5A shows C_m and C_s , derived from the CV data for different TPs. The dependence of capacitance on scan rate for TP 1 (Figure 5A(a)) shows a maximum at 20 mV s^{-1} . It is suggested that the electrode activation during cycling at lower scan rates resulted in the capacitance increase.

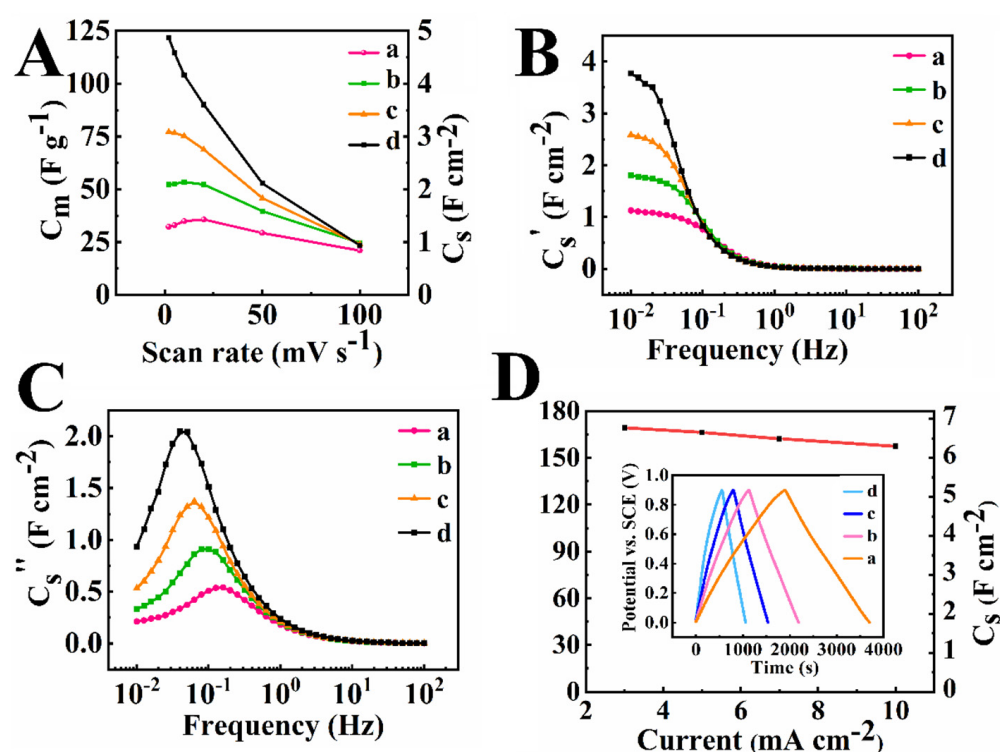


Figure 5. (A) Integral capacitances calculated from the CV data, (B) real and (C) imaginary components of differential complex capacitances versus frequency, calculated from the EIS data for (a) TP 1, (b) TP 2, (c) TP 3, and (d) TP 5; (D) integral capacitance obtained from the GCD data after TP 5 versus current density; inset shows corresponding charge discharge curves for current densities of (a) 3, (b) 5, (c) 7, and (d) 10 mA cm^{-2} .

However, the capacitance decreased at scan rates of 50 and 100 mV s^{-1} , resulting in a maximum (Figure 5A(a)). The capacitance increased with increasing TP number from 1 to 5 (Figure 5). The highest integral capacitance of 4.87 F cm^{-2} (121.8 F g^{-1}) was achieved at 2 mV s^{-1} for TP 5. The components of the differential complex capacitance, obtained

from the EIS data, showed significant variations for TP 1–5 (Figure 5B,C). The frequency dependences of the capacitance components showed relaxation-type [46] dispersions. The real part of the differential complex capacitance increased with increasing TP number in agreement with the CV data. The GCD data obtained after TP 5 showed linear charge–discharge behavior, indicating good capacitive performance (Figure 5D). The integral capacitance of 6.77 F cm^{-2} (169.3 F g^{-1}) was obtained at a current density of 3 mA cm^{-2} . The capacitance slightly decreased with increasing current density and showed good capacitance retention.

Testing of the electrodes prepared by method 2 showed reduced capacitance variations during cycling, and significantly higher capacitances were obtained compared to method 1. Figure 6 compares CV data for TP 1 and TP 3. The areas of CVs increased from TP 1 to TP 3 only at low scan rates. At scan rates of 20 mV s^{-1} and higher, the CV areas were nearly similar for TP1 and TP3. The CV areas for TP 4 and TP 5 were practically the same as for TP 3 for all scan rates.

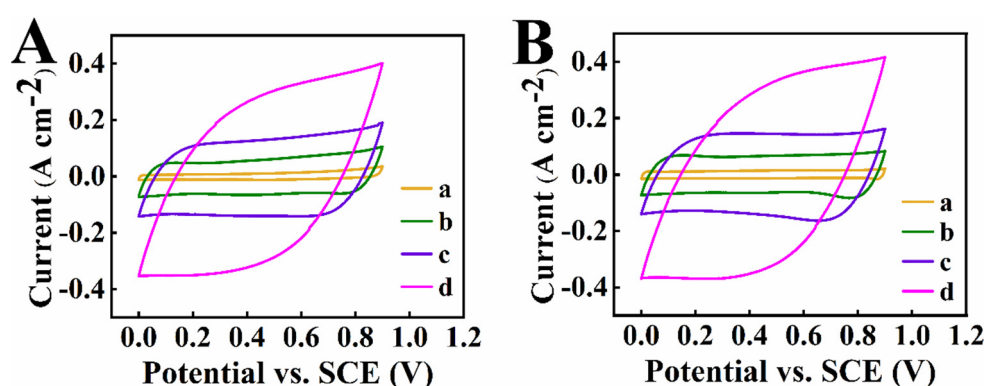


Figure 6. CVs for electrode prepared by Method 2 for (A) TP 1 and (B) TP 3 for scan rates of (a) 2, (b) 10, (c) 20, and (d) 50 mV s^{-1} .

Figure 7A shows integral capacitances, calculated from the CV data for the electrode prepared by Method 2. The capacitance for TP 1 (Figure 7A(a)) showed a maximum for a scan rate of 10 mV s^{-1} . A similar maximum was observed for TP 1 for the electrode prepared by method 1 (Figure 5A(a)). As pointed out above, such a maximum resulted from the activation of the electrode by cycling at low scan rates. Therefore, some activation occurred for the electrodes prepared by Method 2. However, it should be noted that the capacitance obtained for the first cycle at 2 mV s^{-1} for TP 1 for electrode prepared by Method 2 was 5.46 F cm^{-2} (136.4 F g^{-1}), which is higher than the capacitance of 4.87 F cm^{-2} (121.8 F g^{-1}) at 2 mV s^{-1} for TP 5 for the electrode prepared by Method 1. The highest capacitance of 6.67 F cm^{-2} (166.7 F g^{-1}) was achieved at 2 mV s^{-1} for TP 3 for the electrode prepared by Method 2. Turning again to the data presented in Figure 7A, it is seen that very small variations in the capacitance were observed for TP1 and TP3 for scan rates of 20 – 100 mV s^{-1} . The capacitance measurements at different scan rates for TPs 3–5 did not show significant variations in capacitances.

The results of capacitance measurements from the EIS data (Figure 7B,C) correlated with the results obtained by CV. The real part of capacitance for TP 1 at 10 mHz for the electrode prepared by Method 2 was 4.75 F cm^{-2} (118.8 F g^{-1}), which is higher than the capacitance of 3.77 F cm^{-2} (94.25 F g^{-1}) for the electrode prepared by Method 1 at the same frequency and TP 5. The analysis of EIS data for TP 1 and TP 3 revealed changes in both real and imaginary capacitance, which indicates that some activation process occurs for the electrodes prepared by Method 2. The highest real part of the capacitance obtained at 10 mHz for TP 3 for the electrode prepared by Method 2 was found to be 5.70 F cm^{-2} (142.5 F g^{-1}). EIS capacitance data did not show significant variation for TP 4 and TP 5 compared to TP 3.

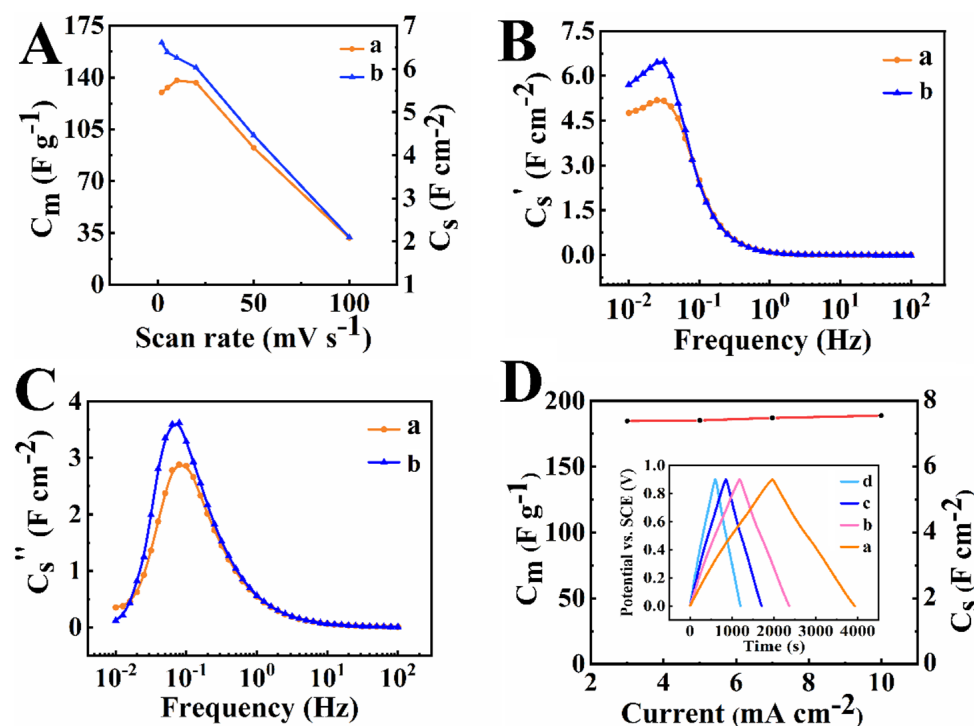


Figure 7. (A) Integral capacitances calculated from the CV data, (B) real and (C) imaginary components of differential complex capacitances versus frequency, calculated from the EIS data for (a) TP 1, (b) TP 3; (D) integral capacitance obtained from the GCD data after TP 5 versus current density; inset shows corresponding charge discharge curves for current densities of (a) 3, (b) 5, (c) 7, and (d) 10 mA cm⁻².

The results of CV and EIS data indicate that Method 2 resulted in a significant acceleration of the activation process. This can potentially eliminate the need in the time-consuming activation process for Mn₃O₄-based electrodes. Indeed, relatively small variations in capacitance were obtained for the electrodes prepared by Method 2. The first cycle of capacitance measurements for the electrodes prepared by this method showed higher capacitance than that for TP 5 for the electrode prepared by Method 1. Turning again to the comparison of MnO₂ and Mn₃O₄ electrodes, it should be noted that some activation process was also reported for the MnO₂ electrodes, which also exhibited a small increase in the capacitance during initial cycling [47]. Such a capacitance increase in the MnO₂ electrodes was attributed to the microstructure changes during initial cycling [47]. GCD testing of the electrodes prepared by Method 2 showed linear charge–discharge curves (Figure 7D), indicating good capacitive behavior. The capacitance of 7.55 F cm⁻² (188.8 F cm⁻²) was achieved at a current density of 3 mA cm⁻². The electrodes prepared by Method 2 showed energy density of 18.8 Wh kg⁻¹ at power density of 0.11 kW kg⁻¹.

In order to analyze the difference in the activation of electrodes prepared by methods 1 and 2, CV studies were performed for fresh electrodes at a scan rate of 50 mV s⁻¹ for 2000 cycles, and the obtained capacitances were normalized by the capacitance obtained for the 2000th cycle (Figure 8).

The normalized capacitance C_N for the first cycle for the electrode prepared by method 1 was only 23% and it was slowly increased with cycle numbers. In contrast, the capacitance for the first cycle for the electrode prepared by Method 2 was 70% and rapidly increased with an increasing cycle number. The comparison with the data presented in Figure 7 also indicates that a lower scan rate can result in a faster activation process for the electrodes prepared by Method 2.

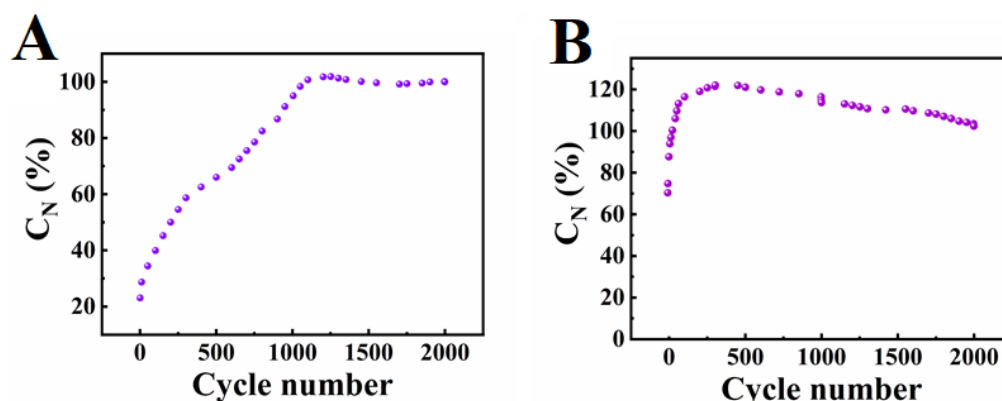


Figure 8. Normalized capacitances (C_N) versus cycle number at a scan rate of 50 mV s^{-1} for electrodes prepared by (A) Method 1 and (B) Method 2, normalized by the capacitance for the 2000th cycle.

The capacitances obtained from CV, EIS, and GCD data for electrodes prepared by Method 2 are significantly higher than the capacitances obtained by the same testing techniques for electrodes prepared by Method 1. The results of this investigation indicated that the use of murexide as a capping agent allowed for an enhanced performance of the Mn_3O_4 -MWCNT electrodes. It should be noted that MWCNTs have a low electrical double-layer-type specific capacitance [48] of about 20 F g^{-1} . The use of MWCNTs as conductive additives is critically important for the utilization of capacitive properties of Mn_3O_4 , which has low conductivity. Due to small MWCNT content in the Mn_3O_4 -MWCNT electrode material, the high capacitance of the composite electrodes resulted from pseudocapacitive properties of Mn_3O_4 .

A recent comprehensive review [6] summarized capacitances for Mn_3O_4 and MnO_2 electrodes with high active mass reported in the literature. A comparison with the literature data for Mn_3O_4 showed that the areal capacitance of Mn_3O_4 -MWCNT electrodes achieved in this investigation is significantly higher than in the literature data (Table 1). Moreover, the capacitance of the Mn_3O_4 -MWCNT electrodes was higher than the capacitances of MnO_2 -MWCNT electrodes of a similar mass reported in the literature (Table 1).

Table 1. Literature data on capacitances of Mn_3O_4 - and MnO_2 -based electrodes containing conductive additives and tested in Na_2SO_4 electrolyte.

Material	Active Mass (mg cm^{-2})	Areal Capacitance (F cm^{-2})	Reference
Mn_3O_4	28.4	2.8	[35]
Mn_3O_4	30.4	2.63	[49]
Mn_3O_4	33.0	4.2	[33]
Mn_3O_4	35.0	3.5	[31]
Mn_3O_4	36.0	3.1	[50]
Mn_3O_4	36.0	3.79	[51]
Mn_3O_4	40.1	4.3	[52]
Mn_3O_4	40.0	6.67	this work
MnO_2	40.0	5.26	[53]
MnO_2	40.0	5.3	[54]
MnO_2	40.0	5.9	[55]
MnO_2	40.0	6.2	[56]

Therefore, the results of this investigation indicate that Mn_3O_4 is a promising alternative to MnO_2 as a cathode material for asymmetric supercapacitors. The strategy developed in this investigation opens up an avenue for a further improvement of capacitive properties of Mn_3O_4 -based electrodes. Of particular importance for future investigations is the ability of Mn_3O_4 to form solid solutions with other spinel compounds. The fabrication and testing of such solid solutions can result in electrodes with higher capacitive properties, which can be combined with improved magnetic and other functional properties.

4. Conclusions

For the first time, murexide was used as a capping agent for the synthesis of Mn_3O_4 nanoparticles and as a co-dispersant for Mn_3O_4 and MWCNTs. The adsorption of murexide on Mn_3O_4 and MWCNTs involved two different mechanisms and facilitated electrostatic co-dispersion of Mn_3O_4 with MWCNTs and their enhanced mixing. The use of murexide as a capping agent in Method 2 allowed for a reduced agglomeration. As a result, the capacitance of the Mn_3O_4 -MWCNT electrodes prepared by Method 2 was significantly higher than the capacitance of the Mn_3O_4 -MWCNT electrodes prepared by Method 1. The simple approach developed in this investigation resulted in record-high capacitances of 6.67 F cm^{-2} obtained from cyclic voltammetry data at a scan rate of 2 mV s^{-1} and 7.55 F cm^{-2} obtained from the galvanostatic charge-discharge data at a current density of 3 mA cm^{-2} . The good electrochemical performance was achieved at a high active mass loading of 40 mg cm^{-2} . It was found that the time-consuming electrode activation procedure for Mn_3O_4 electrodes can be avoided. The approach developed in this investigation paved the way for the development of advanced cathodes for asymmetric supercapacitors for operation in a neutral electrolyte. It is expected that future progress in the fabrication of Mn_3O_4 electrodes will result in a superior performance compared to MnO_2 electrodes for practical applications. Further development of chelating dispersants offers a promising strategy for the synthesis and the colloidal processing of advanced energy storage materials. The ability to achieve high capacitance for a spinel material in a neutral electrolyte opens the door for the fabrication of multifunctional devices, combining capacitive, magnetic, and other functional properties.

Author Contributions: Conceptualization, W.Y. and I.Z.; methodology, W.Y. and M.N.; software, W.Y.; validation, W.Y. and I.Z.; formal analysis, W.Y.; investigation, W.Y.; resources, M.N. and I.Z.; data curation, W.Y.; writing—original draft preparation, W.Y., M.N. and I.Z.; writing—review and editing, W.Y. and I.Z.; visualization, W.Y.; supervision, I.Z.; project administration, I.Z.; funding acquisition, I.Z. All authors have read and agreed to the published version of the manuscript.

Funding: This research was funded by the Natural Sciences and Engineering Research Council of Canada grant number RGPIN-2018-04014 and CRC program. Wenjuan Yang received a scholarship from the China Scholarship Council.

Data Availability Statement: The data presented in this study are available in: “Facile Route for Fabrication of Ferrimagnetic Mn_3O_4 Spinel Material for Supercapacitors with Enhanced Capacitance”.

Acknowledgments: SEM investigations were performed at the Canadian Centre for Electron Microscopy.

Conflicts of Interest: The authors declare no conflict of interest.

References

1. Xiong, C.; Li, B.; Lin, X.; Liu, H.; Xu, Y.; Mao, J.; Duan, C.; Li, T.; Ni, Y. The recent progress on three-dimensional porous graphene-based hybrid structure for supercapacitor. *Compos. Part B Eng.* **2019**, *165*, 10–46. [[CrossRef](#)]
2. Liu, C.; Hou, Y.; Li, Y.; Xiao, H. Heteroatom-doped porous carbon microspheres derived from ionic liquid-lignin solution for high performance Supercapacitors. *J. Colloid Interface Sci.* **2022**, *614*, 566–573. [[CrossRef](#)] [[PubMed](#)]
3. Zhang, H.; Bai, Y.; Chen, H.; Wu, J.; Li, C.M.; Su, X.; Zhang, L. Oxygen-defect-rich 3D porous cobalt-gallium layered double hydroxide for high-performance supercapacitor application. *J. Colloid Interface Sci.* **2022**, *608*, 1837–1845. [[CrossRef](#)] [[PubMed](#)]
4. Yan, Q.; Cheng, Y.; Wang, R.; Sun, J. Recent advances in 3D porous MXenes: Structures, properties and applications. *J. Phys. D Appl. Phys.* **2021**, *55*, 093001. [[CrossRef](#)]
5. Wang, T.; He, X.; Gong, W.; Kou, Z.; Yao, Y.; Fulbright, S.; Reardon, K.F.; Fan, M. Three-dimensional, heteroatom-enriched, porous carbon nanofiber flexible paper for free-standing supercapacitor electrode materials derived from microalgae oil. *Fuel Process. Technol.* **2022**, *225*, 107055. [[CrossRef](#)]
6. Chen, R.; Yu, M.; Sahu, R.P.; Puri, I.K.; Zhitomirsky, I. The Development of Pseudocapacitor Electrodes and Devices with High Active Mass Loading. *Adv. Energy Mater.* **2020**, *10*, 1903848. [[CrossRef](#)]
7. Gogotsi, Y.; Anasori, B. The rise of MXenes. *ACS Nano* **2019**, *13*, 8491–8494. [[CrossRef](#)]
8. Huang, T.; Cui, W.; Qiu, Z.; Hu, Z.; Zhang, Z. 2D porous layered NiFe_2O_4 by a facile hydrothermal method for asymmetric supercapacitor. *Ionics* **2021**, *27*, 1347–1355. [[CrossRef](#)]

9. Gao, X.; Wang, W.; Bi, J.; Chen, Y.; Hao, X.; Sun, X.; Zhang, J. Morphology-controllable preparation of NiFe₂O₄ as high performance electrode material for supercapacitor. *Electrochim. Acta* **2019**, *296*, 181–189. [[CrossRef](#)]
10. Nawwar, M.; Sahu, R.P.; Puri, I.K.; Zhitomirsky, I. Pseudocapacitive behavior of ferrimagnetic NiFe₂O₄-carbon nanotube electrodes prepared with a multifunctional dispersing agent. *Open Ceram.* **2021**, *6*, 100127. [[CrossRef](#)]
11. Wang, C.; Zhou, E.; He, W.; Deng, X.; Huang, J.; Ding, M.; Wei, X.; Liu, X.; Xu, X. NiCo₂O₄-based supercapacitor nanomaterials. *Nanomaterials* **2017**, *7*, 41. [[CrossRef](#)]
12. Meena, S.; Anantharaju, K.S.; Malini, S.; Dey, A.; Renuka, L.; Prashantha, S.C.; Vidya, Y.S. Impact of temperature-induced oxygen vacancies in polyhedron MnFe₂O₄ nanoparticles: As excellent electrochemical sensor, supercapacitor and active photocatalyst. *Ceram. Int.* **2021**, *47*, 14723–14740. [[CrossRef](#)]
13. Alshehri, S.M.; Ahmed, J.; Alhabarah, A.N.; Ahamad, T.; Ahmad, T. Nitrogen-Doped Cobalt Ferrite/Carbon Nanocomposites for Supercapacitor Applications. *ChemElectroChem* **2017**, *4*, 2952–2958. [[CrossRef](#)]
14. Nawwar, M.; Poon, R.; Chen, R.; Sahu, R.P.; Puri, I.K.; Zhitomirsky, I. High areal capacitance of Fe₃O₄-decorated carbon nanotubes for supercapacitor electrodes. *Carbon Energy* **2019**, *1*, 124–133. [[CrossRef](#)]
15. Deshmukh, V.V.; Nagaswarupa, H.P.; Raghavendra, N. Development of Co-doped MnFe₂O₄ nanoparticles for electrochemical supercapacitors. *Ceram. Int.* **2021**, *47*, 10268–10273. [[CrossRef](#)]
16. Angelopoulou, P.; Kassavetis, S.; Papavasiliou, J.; Karfaridis, D.; Slowik, G.; Patsalas, P.; Avgouropoulos, G. Enhanced Performance of LiAl_{0.1}Mn_{1.9}O₄ Cathode for Li-Ion Battery via TiN Coating. *Energies* **2021**, *14*, 825. [[CrossRef](#)]
17. Abdel-Ghany, A.; Hashem, A.M.; Mauger, A.; Julien, C.M. Lithium-Rich Cobalt-Free Manganese-Based Layered Cathode Materials for Li-Ion Batteries: Suppressing the Voltage Fading. *Energies* **2020**, *13*, 3487. [[CrossRef](#)]
18. Vu, N.H.; Dao, V.-D.; Tran Huu, H.; Im, W.B. Effect of Synthesis Temperature on Structure and Electrochemical Performance of Spinel-Layered Li_{1.33}MnTiO_{4+z} in Li-Ion Batteries. *Energies* **2020**, *13*, 2962. [[CrossRef](#)]
19. Venevtsev, Y.N.; Gagulin, V.V.; Zhitomirsky, I.D. Material science aspects of seignette-magnetism problem. *Ferroelectrics* **1987**, *73*, 221–248. [[CrossRef](#)]
20. Nawwar, M.; Poon, R.; Sahu, R.P.; Puri, I.K.; Zhitomirsky, I. Fe₃O₄ spinel-Mn₃O₄ spinel supercapacitor prepared using Celestine blue as a dispersant, capping agent and charge transfer mediator. *Ceram. Int.* **2020**, *46*, 18851–18858. [[CrossRef](#)]
21. Guan, D.; Gao, Z.; Yang, W.; Wang, J.; Yuan, Y.; Wang, B.; Zhang, M.; Liu, L. Hydrothermal synthesis of carbon nanotube/cubic Fe₃O₄ nanocomposite for enhanced performance supercapacitor electrode material. *Mater. Sci. Eng. B* **2013**, *178*, 736–743. [[CrossRef](#)]
22. Nipan, G.; Smirnova, M.; Kornilov, D.Y.; Kop'eva, M.; Nikiforova, G.; Gubin, S. Transformation of Solid Solution with Spinel-Type Structure Within the Range LiMn_{2-x}(Ni_{0.33}Co_{0.33}Fe_{0.33})_xO₄ (0 ≤ x ≤ 2). *J. Phase Equilibria Diffus.* **2020**, *41*, 819–826. [[CrossRef](#)]
23. Joo, H.; Lee, J.; Yoon, J. Short Review: Timeline of the Electrochemical Lithium Recovery System Using the Spinel LiMn₂O₄ as a Positive Electrode. *Energies* **2020**, *13*, 6235. [[CrossRef](#)]
24. Abbas, S.M.; Hashem, A.M.; Abdel-Ghany, A.E.; Ismail, E.H.; Kotlár, M.; Winter, M.; Li, J.; Julien, C.M. Ag-Modified LiMn₂O₄ Cathode for Lithium-Ion Batteries: Coating Functionalization. *Energies* **2020**, *13*, 5194. [[CrossRef](#)]
25. Cao, K.; Jia, Y.; Wang, S.; Huang, K.-J.; Liu, H. Mn₃O₄ nanoparticles anchored on carbon nanotubes as anode material with enhanced lithium storage. *J. Alloy. Compd.* **2021**, *854*, 157179. [[CrossRef](#)]
26. Dai, Y.; Men, Y.; Wang, J.; Liu, S.; Li, S.; Li, Y.; Wang, K.; Li, Z. Tailoring the morphology and crystal facet of Mn₃O₄ for highly efficient catalytic combustion of ethanol. *Colloids Surf. A Physicochem. Eng. Asp.* **2021**, *627*, 127216. [[CrossRef](#)]
27. Rizal, M.Y.; Saleh, R.; Taufik, A.; Yin, S. Photocatalytic decomposition of methylene blue by persulfate-assisted Ag/Mn₃O₄ and Ag/Mn₃O₄/graphene composites and the inhibition effect of inorganic ions. *Environ. Nanotechnol. Monit. Manag.* **2021**, *15*, 100408. [[CrossRef](#)]
28. Patil, T.S.; Gangawane, S.A.; Takale, M.V. A Review on Mn₃O₄ and Its Composite Nanomaterials of Diverse Morphologies as an Electrode Material in Supercapacitors. *Int. J. Sci. Res. Sci. Technol.* **2021**, *8*, 520–526.
29. Sayyed, S.G.; Shaikh, A.V.; Dubal, D.P.; Pathan, H.M. Paving the Way towards Mn₃O₄ Based Energy Storage Systems. *ES Energy Environ.* **2021**, *14*, 3–21. [[CrossRef](#)]
30. Rorabeck, K.; Zhitomirsky, I. Salting-out aided dispersive extraction of Mn₃O₄ nanoparticles and carbon nanotubes for application in supercapacitors. *Colloids Surf. A Physicochem. Eng. Asp.* **2021**, *618*, 126451. [[CrossRef](#)]
31. Poon, R.; Zhitomirsky, I. High areal capacitance of Mn₃O₄-carbon nanotube electrodes. *Mater. Lett.* **2018**, *215*, 4–7. [[CrossRef](#)]
32. Nagarajan, N.; Cheong, M.; Zhitomirsky, I. Electrochemical capacitance of MnOx films. *Mater. Chem. Phys.* **2007**, *103*, 47–53. [[CrossRef](#)]
33. Milne, J.; Zhitomirsky, I. Application of octanohydroxamic acid for liquid-liquid extraction of manganese oxides and fabrication of supercapacitor electrodes. *J. Colloid Interface Sci.* **2018**, *515*, 50–57. [[CrossRef](#)]
34. Poon, R.; Liang, W.; Zhitomirsky, I. Mn₃O₄ and (ZnFe) OOH Composites for Supercapacitors with High Active Mass. *Metall. Mater. Trans. A* **2020**, *51*, 855–862. [[CrossRef](#)]
35. Ata, M.S.; Milne, J.; Zhitomirsky, I. Fabrication of Mn₃O₄-carbon nanotube composites with high areal capacitance using cationic and anionic dispersants. *J. Colloid Interface Sci.* **2018**, *512*, 758–766. [[CrossRef](#)] [[PubMed](#)]
36. Stanley, P.M.; Warnan, J. Molecular Dye-Sensitized Photocatalysis with Metal-Organic Framework and Metal Oxide Colloids for Fuel Production. *Energies* **2021**, *14*, 4260. [[CrossRef](#)]
37. Zhang, C.; Zhang, R.; Liu, H.; Wei, Q.; Gong, D.; Mo, L.; Tao, H.; Cui, S.; Wang, L. One-Step Synthesis of Highly Dispersed and Stable Ni Nanoparticles Confined by CeO₂ on SiO₂ for Dry Reforming of Methane. *Energies* **2020**, *13*, 5956. [[CrossRef](#)]

38. Zhitomirsky, I.; Gal-Or, L. Formation of hollow fibers by electrophoretic deposition. *Mater. Lett.* **1999**, *38*, 10–17. [[CrossRef](#)]
39. Lee, S.H.; Woo, S.P.; Kakati, N.; Kim, D.-J.; Yoon, Y.S. A Comprehensive Review of Nanomaterials Developed Using Electrophoresis Process for High-Efficiency Energy Conversion and Storage Systems. *Energies* **2018**, *11*, 3122. [[CrossRef](#)]
40. Ata, M.; Liu, Y.; Zhitomirsky, I. A review of new methods of surface chemical modification, dispersion and electrophoretic deposition of metal oxide particles. *RSC Adv.* **2014**, *4*, 22716–22732. [[CrossRef](#)]
41. Martin, R.L.; White, A.H.; Willis, A.C. Structural studies in metal–purpurate complexes. Part 1. Crystal structures of potassium purpurate trihydrate and ammonium purpurate monohydrate (murexide). *J. Chem. Soc. Dalton Trans.* **1977**, *8*, 1336–1342. [[CrossRef](#)]
42. Masoud, M.; Kassem, T.; Shaker, M.; Ali, A. Studies on transition metal murexide complexes. *J. Therm. Anal. Calorim.* **2006**, *84*, 549–555. [[CrossRef](#)]
43. Zhao, H.; Wang, L.; Qiu, Y.; Zhou, Z.; Zhong, W.; Li, X. Multiwalled carbon nanotubes as a solid-phase extraction adsorbent for the determination of three barbiturates in pork by ion trap gas chromatography–tandem mass spectrometry (GC/MS/MS) following microwave assisted derivatization. *Anal. Chim. Acta* **2007**, *586*, 399–406. [[CrossRef](#)] [[PubMed](#)]
44. Wallar, C.; Poon, R.; Zhitomirsky, I. High Areal Capacitance of V₂O₃-Carbon Nanotube Electrodes. *J. Electrochem. Soc.* **2017**, *164*, A3620–A3627. [[CrossRef](#)]
45. Gogotsi, Y.; Simon, P. True performance metrics in electrochemical energy storage. *Science* **2011**, *334*, 917–918. [[CrossRef](#)] [[PubMed](#)]
46. Shi, K.; Zhitomirsky, I. Fabrication of Polypyrrole-Coated Carbon Nanotubes Using Oxidant–Surfactant Nanocrystals for Supercapacitor Electrodes with High Mass Loading and Enhanced Performance. *ACS Appl. Mater. Interfaces* **2013**, *5*, 13161–13170. [[CrossRef](#)]
47. Rorabeck, K.; Zhitomirsky, I. Dispersant Molecules with Functional Catechol Groups for Supercapacitor Fabrication. *Molecules* **2021**, *26*, 1709. [[CrossRef](#)]
48. Shi, K.; Ren, M.; Zhitomirsky, I. Activated Carbon-Coated Carbon Nanotubes for Energy Storage in Supercapacitors and Capacitive Water Purification. *ACS Sustain. Chem. Eng.* **2014**, *2*, 1289–1298. [[CrossRef](#)]
49. Poon, R.; Zhao, X.; Ata, M.S.; Clifford, A.; Zhitomirsky, I. Phase transfer of oxide particles for application in thin films and supercapacitors. *Ceram. Int.* **2017**, *43*, 8314–8320. [[CrossRef](#)]
50. Milne, J.; Silva, R.M.; Zhitomirsky, I. Surface modification and dispersion of ceramic particles using liquid-liquid extraction method for application in supercapacitor electrodes. *J. Eur. Ceram. Soc.* **2019**, *39*, 3450–3455. [[CrossRef](#)]
51. Poon, R.; Zhitomirsky, I. Application of Cyrene as a solvent and dispersing agent for fabrication of Mn₃O₄-carbon nanotube supercapacitor electrodes. *Colloid Interface Sci. Commun.* **2020**, *34*, 100226. [[CrossRef](#)]
52. Rorabeck, K.; Zhitomirsky, I. Application of Octanohydroxamic Acid for Salting out Liquid–Liquid Extraction of Materials for Energy Storage in Supercapacitors. *Molecules* **2021**, *26*, 296. [[CrossRef](#)] [[PubMed](#)]
53. Liu, Y.; Zhitomirsky, I. Aqueous electrostatic dispersion and heterocoagulation of multiwalled carbon nanotubes and manganese dioxide for the fabrication of supercapacitor electrodes and devices. *RSC Adv.* **2014**, *4*, 45481–45489. [[CrossRef](#)]
54. Liu, Y.; Shi, K.; Zhitomirsky, I. New colloidal route for electrostatic assembly of oxide nanoparticle–carbon nanotube composites. *Colloids Surf. A Physicochem. Eng. Asp.* **2014**, *446*, 15–22. [[CrossRef](#)]
55. Wang, Y.; Liu, Y.; Zhitomirsky, I. Surface modification of MnO₂ and carbon nanotubes using organic dyes for nanotechnology of electrochemical supercapacitors. *J. Mater. Chem. A* **2013**, *1*, 12519–12526. [[CrossRef](#)]
56. Li, J.; Yang, Q.M.; Zhitomirsky, I. Nickel foam-based manganese dioxide–carbon nanotube composite electrodes for electrochemical supercapacitors. *J. Power Sources* **2008**, *185*, 1569–1574. [[CrossRef](#)]